ACS APPLIED MATERIALS & INTERFACES

Research Article

www.acsami.org

Organically Modified Saponites: SAXS Study of Swelling and Application in Caffeine Removal

Liziane Marçal,[†] Emerson H. de Faria,*[,†] Eduardo J. Nassar,[†] Raquel Trujillano,[‡] Nuria Martín,[‡] Miguel A. Vicente,[‡] Vicente Rives,[‡] Antonio Gil,[£] Sophia A. Korili,[£] and Katia J. Ciuffi*[,†]

[†]Universidade de Franca, Avenida Dr. Armando Salles Oliveira, Parque Universitário, 201, 14404−600, Franca/SP, Brazil

[‡]GIR−QUESCAT, Departamento de Química Inorgánica, Universidad de Salamanca, 37008 Salamanca, Spain

[£]Departamento de Química Aplicada, Universidad Pública de Navarra, 31006 Pamplona, Spain

ABSTRACT: This study aimed to assess the capacity of saponite modified with n-hexadecyltrimethylammonium bromide (CTAB) and/or 3-aminopropyltriethoxysilane (APTS) to adsorb and remove caffeine from aqueous solutions. Powder X-ray diffraction (PXRD) revealed increased basal spacing in the modified saponites. Small-angle X-ray scattering (SAXS) confirmed the PXRD results; it also showed how the different clay layers were stacked and provided information on the swelling of natural saponite and of the saponites functionalized with CTAB and/or APTS. Thermal analyses, infrared spectroscopy, scanning electron microscopy, element chemical analysis, and textural analyses confirmed functionalization of the natural saponite. The maximum adsorption capacity at equilibrium was 80.54 mg/g, indicating that the saponite modified with 3-aminopropyltriethoxysilane constitutes an efficient and suitable caffeine adsorbent.

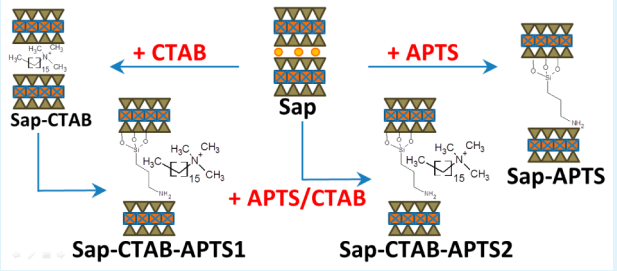

KEYWORDS: *saponite, organoclay, caffeine adsorption, emerging contaminants, wastewater*

INTRODUCTION

The so-called emerging contaminants (pharmaceuticals, steroids and hormones, personal care products, antiseptics, surfactants and surfactant metabolites, flame retardants, industrial additives and agents, gasoline additives, and disinfection byproducts, among others) have arisen in wastewater treatment plant effluents over recent years. Conventional treatment technologies cannot completely remove these substances, which can accumulate and become a potential threat to human health and aquatic animals.[1] Particularly important pharmaceutical contaminants include clofibric acid, diclofenac, caffeine, and salicylic acid.[2]

Caffeine (1,3,7-trimethylxanthine) is an alkaloid belonging to the methylxanthine family; this compound has found wide application as stimulant. Large amounts of caffeine occur in the seeds, leaves, and fruits of some plants. Therein, caffeine acts as a natural pesticide that paralyzes and kills certain insects that feed on these plants. Humans most commonly consume caffeine in infusions extracted from coffee plant seeds and tea bush leaves as well as in various foods and drinks containing products derived from the kola nut. In humans, caffeine acts as a central nervous system stimulant, temporarily warding off drowsiness and restoring alertness. Ordinary caffeine consumption poses low risks to the human health. In fact, caffeine consumption over the years may exert a modest protective effect against a number of diseases, like Parkinson's disease, heart disease, and certain types of cancer.[3]

Regular consumption worldwide has made caffeine a chemical marker of surface water pollution. The fact that wastewater microorganisms cannot metabolize this compound satisfactorily has suggested that caffeine can serve as a chemical indicator of environmental pollution. In humans, hepatic cytochrome P450 partially metabolizes dietary caffeine via oxidative N-demethylation and/or ring oxidation, to produce theophylline (1,3-dimethylxanthine), paraxanthine (1,7-dimethylxanthine), 1,3,7-trimethyluric acid, and other byproducts. The products and byproducts of caffeine metabolism are excreted in the urine together with non-degraded caffeine.[4,5] Unfortunately, wastewater treatment plants are not generally designed to treat small quantities of these molecules, which calls for their removal from effluents before wastewater purification processes.

Several technologies can improve the removal of emerging pollutants from aqueous solutions.[6] Among non-destructive technologies, coagulation−flocculation, membrane separation, and ion exchange and adsorption are worthy of mention. Although adsorption processes can remove an array of organic pollutants from aqueous solutions,[7] higher efficiencies are still necessary. In this sense, it is crucial to determine which factors enhance the separation of these pollutants from aqueous medium and to develop materials that display the desirable removal properties. Sotelo et al. have investigated caffeine removal via adsorption onto various carbon materials and found an adsorption capacity of 270 mg/g.[8−10] Cabrera−Lafauri et al.[11,12]

Received: March 3, 2015
Accepted: May 1, 2015
Published: May 4, 2015

DOI: 10.1021/acsami.5b01894
ACS Appl. Mater. Interfaces 2015, 7, 10853−10862

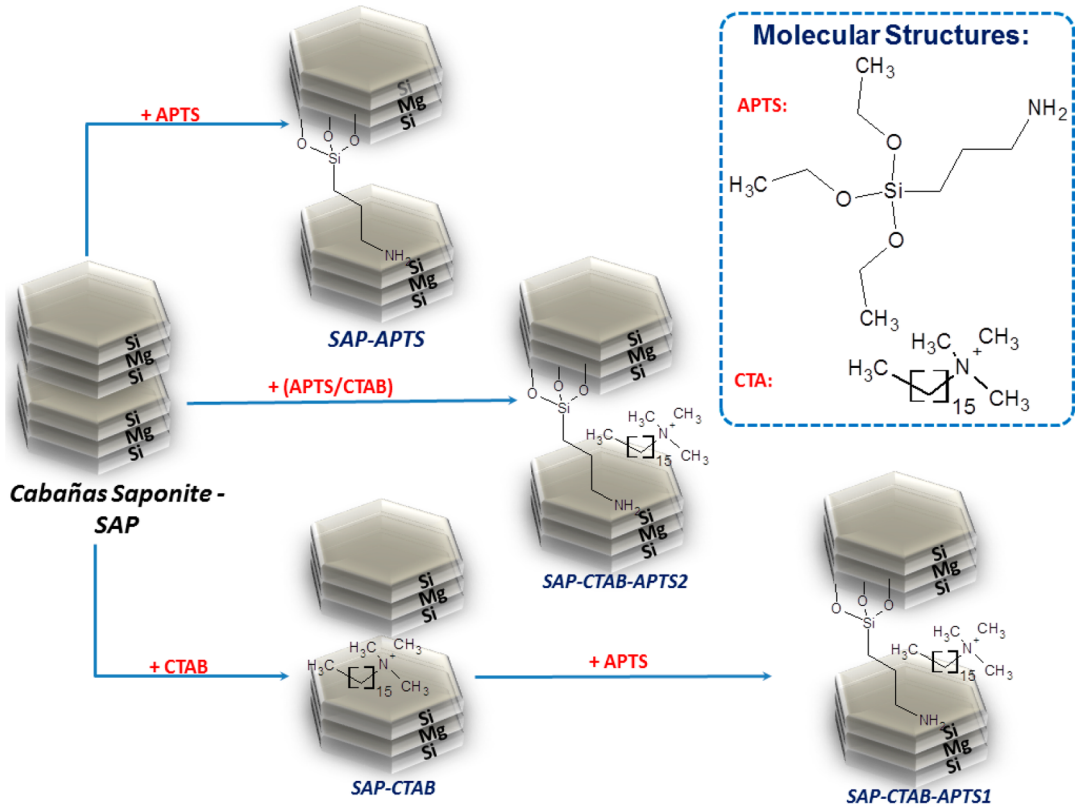

Figure 1. Schematic representation of saponite derivatives intercalated and/or grafted with CTAB and APTS.

verified that in the presence of Co, Cu, and Ni, inorganic–organic pillared clays had increased capacity to remove caffeine. Okada et al.[13] have recently reported increased and decreased caffeine uptake by clays functionalized with benzylamine hydrochloride and neostigmine bromide, respectively.

This work reports on the use of an organofunctionalized saponite to adsorb caffeine from aqueous solutions. To this end, we functionalized saponite with the surfactant *n*-hexadecyltrimethylammonium bromide (CTAB) and/or with the alkoxysilane 3-aminopropyltriethoxysilane (APTS) and investigated how clay funcionalization affected the capacity of saponite to adsorb caffeine.

EXPERIMENTAL SECTION

Starting Materials. The saponite used in this work came from the Cabañas deposit (Spain) and was kindly supplied by TOLSA. Natural saponite was purified by the dispersion–decantation method. The fraction with particle size below 2 μm, composed of very pure saponite, was selected.[14]

Intercalation of the Surfactant CTAB into Saponite. A portion of 3.0 g of purified saponite was suspended in 50 cm^3 of distilled water/acetone (2:1, v/v). Then, a solution of 2.1 g of *n*-hexadecyltrimethylammonium bromide (CTAB) in 50 cm^3 of distilled water was slowly added to the suspended clay, and the mixture magnetically stirred at 50 °C for 24 h. The solid was separated by centrifugation and washed with distilled water and ethanol, to remove the non-attached surfactant. The final material (SAP–CTAB) was dried at 60 °C.

Saponite Functionalization with the Alkoxysilane APTS. A suspension containing 3.0 g of purified saponite in 35 cm^3 of distilled water/ethanol (2:1, v/v) was prepared. Then, 1.4 cm^3 of 3-aminopropyltriethoxysilane (abbreviated APTS herein, although sometimes it is also abbreviated as APTES in the literature) and 0.25 cm^3 of concentrated hydrochloric acid were added to the suspension, and the mixture was magnetically stirred at room temperature for 24 h. The solid was separated by centrifugation and washed with distilled water; the final material was dried at 60 °C and labeled as SAP–APTS.

Simultaneous Saponite Functionalization with CTAB and APTS. For comparison, two additional samples were prepared. One sample, designated SAP–CTAB–APTS1, was obtained by adding APTS to SAP–CTAB prepared as described above. The other sample, designated SAP–CTAB–APTS2, was achieved by simultaneously adding both CTAB and APTS to the saponite. After 24 h of reaction at room temperature, the solids were separated by centrifugation, washed with water and ethanol, and dried at 60 °C. The schematic representation of the various methodologies followed herein and of the samples obtained in this work is included in Figure 1.

Characterization Techniques. The powder X-ray diffractograms (PXRD) of the solids were recorded on a Siemens D-500 diffractometer operating at 40 kV and 30 mA (1200 W); filtered Cu Kα radiation was employed. The angle 2θ varied from 2 to 65°. All the analyses were undertaken at a scan rate of 2° (2θ) per minute.

The materials nanostructure was monitored by small-angle X-ray scattering (SAXS) experiments performed at the D01A–SAXS2 beamline of the National Synchrotron Light Laboratory (LNLS, Campinas, Brazil). A vertical position-sensitive X-ray detector and a multichannel analyzer were used to record the SAXS intensity, $I(q)$, as a function of the modulus of the scattering vector $q = (4\pi/\lambda)\sin(\theta/2)$, where θ corresponds to the scattering angle and λ is the wavelength of the X-ray beam (λ = 0.148 nm). The distance between the sample and the detector was 700 mm; 3 s was necessary for each data collection. The beam center was calibrated using silver behenate with the primary reflection peak at 1.076 nm^{-1}. Natural saponite and the grafted/intercalated derivatives under fixed concentration of 10 g/dm^3 were analyzed in the swelling experiment. The clay suspension was placed in a metal SAXS cell holder fitted with a mica window with an internal diameter of 1 cm and thickness of 1 mm. The data acquisition time was about 60 min depending on the sample concentration and on the scattering vector range. The background scattering of a blank (SAXS holder with mica) was subtracted from the spectrum of each sample before further data analysis was carried out for the saponite systems.

DOI: 10.1021/acsami.5b01894
ACS Appl. Mater. Interfaces 2015, 7, 10853–10862

The thermal analyses were conducted on a TA Instruments SDT Q600 simultaneous DTA–TGA thermal analyzer, in the 25–1000 °C temperature range, at a heating rate of 20 °C/min and under airflow of 100 cm^3/min.

The FTIR infrared absorption spectra were registered on a Perkin–Elmer 1739 spectrometer equipped with a He–Ne laser radiation source (λ = 632.8 nm) and Spectrum for Windows software. The KBr pellet technique was used; the sample/KBr mass ratio was close to 1:300, pressing occurred at 8 T/cm^2. The spectra were recorded between 4000–400 cm^{-1}, with a nominal resolution of 4 cm^{-1}. To improve the signal-to-noise ratio, were took 16 scans.

Scanning electron microscopy (SEM) of the materials was performed on a Carl Zeiss SEM EVO HD25 microscope at the Spanish Pulsed Laser Center (CLPU, Salamanca). The samples were coated with a thin gold layer by using a Bio–Rad ES100 SEN coating system.

Elemental chemical analysis was conducted by atomic absorption on a Mark II ELL–240 Instrument in Servicio General de Análisis Químico Aplicado (Universidad de Salamanca, Spain).

The textural analyses were accomplished from the corresponding N_2 adsorption isotherms at −196 °C, obtained in a static volumetric apparatus (Micromeritics model ASAP 2020 adsorption analyzer). The samples (0.2 g) were degassed at 150 °C for 24 h. The specific surface area (S_{BET}) was obtained by the BET method, and the total pore volume was calculated from the amount of N_2 adsorbed at a relative pressure of 0.95.

The cationic exchange capacity (CEC) was calculated by adsorption of methylene blue (MB), which also allowed determination of the specific surface area accessible to this molecule (SSA). The MB solution was prepared by dissolving 1 g of dry MB powder in 200 cm^3 of distilled water. Next, 50 mg of oven-dried samples was suspended in 10 cm^3 of distilled water, and the MB solution was added to this sample suspension in 0.5 cm^3 aliquots. After addition of each 0.5 cm^3 aliquot, the suspension was homogenized by magnetic stirring for 1 min. Then, a small drop was removed from the solution and placed onto Fisher brand filter paper. The fact that nonadsorbed MB formed a permanent blue halo around the suspension aggregate spot on the filter paper meant that MB replaced cations in the double layer and coated the entire surface. The cation exchange capacity was determined from the amount of MB required to reach the end point, according to the following equation

$$\mathrm{CEC} = \frac{[\mathrm{MB}]V}{W} \tag{1}$$

where CEC is the cation exchange capacity (mequiv/100 g), [MB] is the concentration of the methylene blue solution (mequiv/dm^3), V is the volume of the MB solution used during the assay, and W (g) is the mass of solid used in the experiment.

The specific surface area accessible to MB (SSA) was calculated according to Hang and Brindley,[15] and Macek et al.[16] This method assumes that MB molecules cover the particle surface area, and that the MB molecule approximates a rectangle with a surface area of 130 $Å^2$/molecule. From the amount of adsorbed MB, expressed as CEC (eq 1), the SSA was calculated by means of eq 2

$$\mathrm{SSA} = F_{\mathrm{MB}}\mathrm{CEC} \tag{2}$$

where SSA is the accessible specific surface area (m^2/g), F_{MB} is a constant based on the approximated MB area, with a value 7.8043 (m^2/mequiv), and CEC is the cation exchange capacity (mequiv/100 g).

Adsorption Experiments. UV–visible spectroscopy on a Hewlett–Packard 8453 Diode Array spectrometer helped to determine caffeine concentration (Sigma–Aldrich) in the solutions. Absorption was measured at 274 nm, which corresponded to the maximum absorbance of the molecule under the adsorption conditions. Calibration had been previously carried out with caffeine solutions at concentrations ranging between 1 and 10 ppm. According to the Beer–Lambert law, absorbance at this wavelength showed a linear response in all the concentration range used in the experiments.

The adsorption kinetics experiments were carried out in glass vials by shaking a known amount of the adsorbent (SAP–CTAB, SAP–APTS, SAP–CTAB–APTS1, or SAP–CTAB–APTS2), typically 50 mg, with 5.0 cm^3 of an aqueous caffeine solution at a concentration of 20 ppm. The suspensions were then continuously stirred at room temperature. At pre–determined time intervals (between 0.5 and 300 min), the caffeine concentration in the supernatant was analyzed, and the amount of caffeine adsorbed onto the solid was calculated according to eq 3

$$q_t = \frac{V(C_{\mathrm{i}} - C_t)}{m} \tag{3}$$

where q_t (mg/g) is the amount of caffeine adsorbed at time t (min), C_i (mg/dm^3) is the initial caffeine concentration in the solution, C_t (mg/dm^3) is the caffeine concentration in the solution at time t, V (dm^3) is the volume of the solution, and m (g) is the amount of adsorbent.

The adsorption equilibrium experiments were carried out in glass vials, at 25 °C, by shaking a known amount of the adsorbent, typically 50 mg, with 5.0 cm^3 of caffeine solution at the desired concentration, typically between 10 and 800 ppm. The vials containing the caffeine solution and the adsorbent were shaken for 4 h. Then, the clay was separated from the supernatant by centrifugation at 3500 rpm for 15 min. UV–vis spectroscopy at 274 nm helped to determine the concentration of caffeine that remained in the supernatant; the amount of adsorbed dye was calculated according to eq 4

$$q_{\mathrm{e}} = \frac{V(C_{\mathrm{i}} - C_{\mathrm{e}})}{m} \tag{4}$$

where q_e is the amount of adsorbed caffeine (mg/g), C_i and C_e (mg/dm^3) are the initial and equilibrium liquid–phase concentrations of caffeine, respectively, V is the volume of the solution (dm^3), and m is the amount of adsorbent (g).

Theoretical Approach. To fit the data concerning the equilibrium of caffeine adsorption onto organically modified saponites, we employed the Freundlich, Langmuir, and Sips isotherm models.

Freundlich Isotherm. The Freundlich equation is an empirical equation used to describe heterogeneous systems. It is usually written as[17]

$$q_{\mathrm{e}} = k_{\mathrm{F}} C_{\mathrm{e}}^{1/m_{\mathrm{F}}} \tag{5}$$

where k_F and m_F are empirical constants that represent the extent of adsorption and its efficacy, respectively.

Langmuir Isotherm. The Langmuir adsorption model predicts that a monolayer covers the adsorbate at the outer surface of the adsorbent; adsorption takes place at specific homogeneous sites of the adsorbent surface, which implies that all adsorption sites are identical and energetically equivalent.

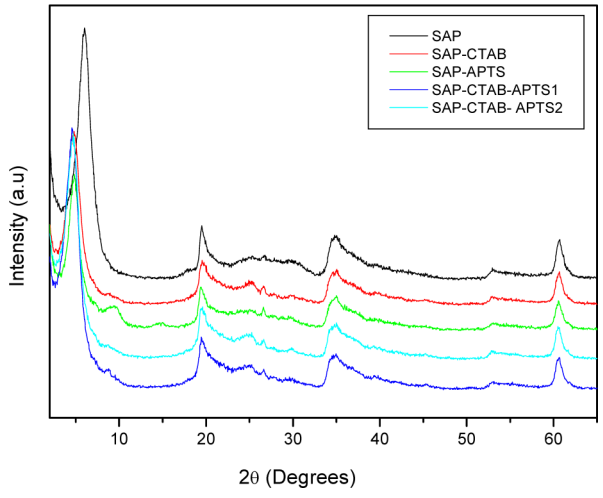

Figure 2. X-ray powder diffraction patterns of the original saponite and of the saponite after functionalization with APTS and/or CTAB.

DOI: 10.1021/acsami.5b01894
ACS Appl. Mater. Interfaces 2015, 7, 10853–10862

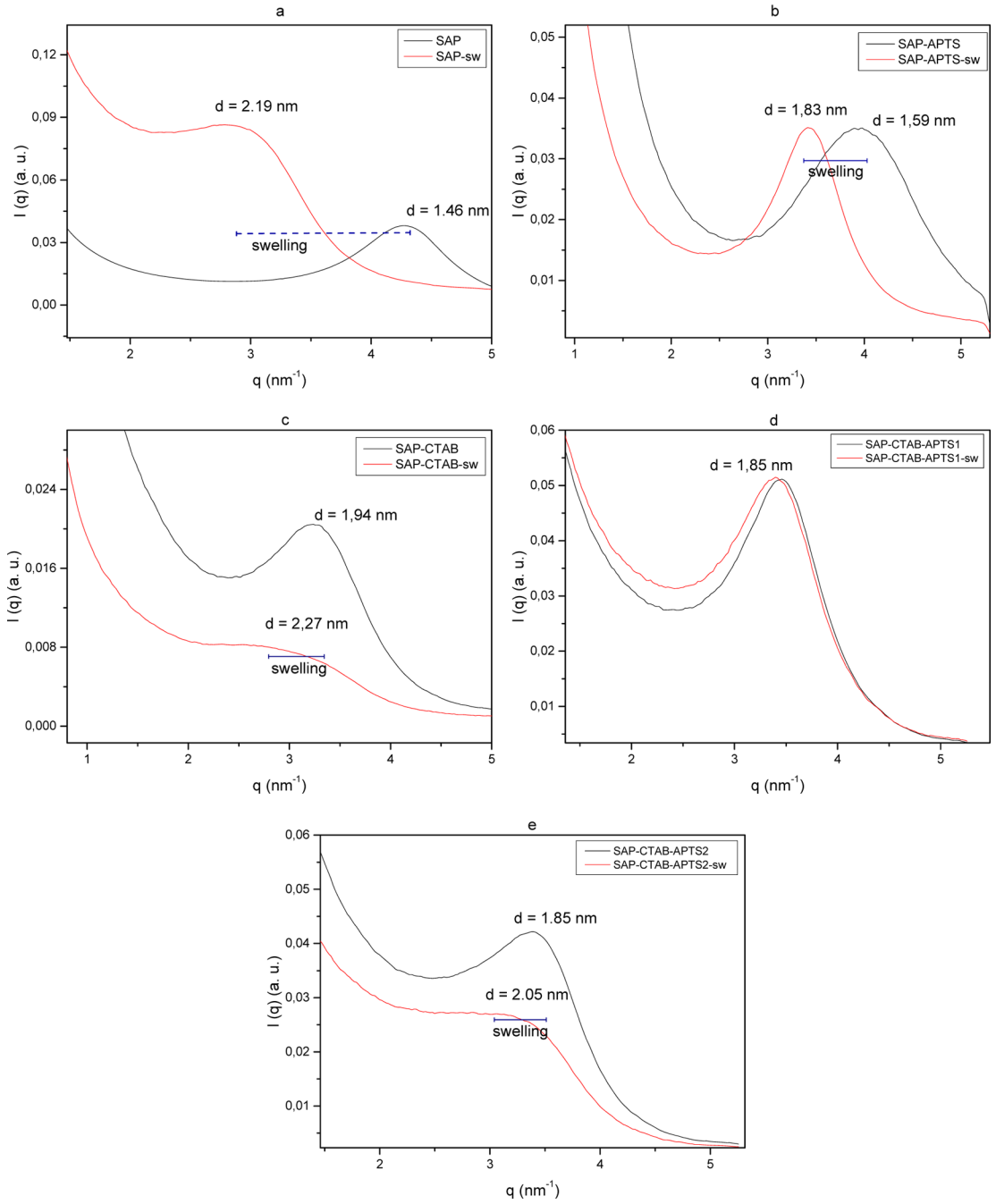

Figure 3. SAXS results for saponite and its functionalized derivatives before and after swelling experiments in aqueous suspension: (a) natural saponite, (b) SAP−APTS, (c) SAP−CTAB, (d) SAP−APTS−CTAB1, and (e) SAP−APTS−CTAB2. ("−sw" designates the samples submitted to swelling experiments).

The Langmuir adsorption isotherm has been successfully applied to many adsorption processes involving organic compounds. It can be written as[18]

$$q_e = \frac{q_L k_L C_e}{1 + k_L C_e} \tag{6}$$

where q_L (mg/g) and k_L (dm^3/mg) are Langmuir constants representing the monolayer adsorption capacity.

Sips Isotherm. This model combines the Freundlich and Langmuir model parameters.[19] At low concentrations, the Freundlich model describes the adsorption mechanism, and at high concentrations, the adsorption mechanism resembles the mechanism of the Langmuir model. Thus, the two equations were adjusted and represented as follows

$$q_e = \frac{q_S k_S C_e^{m_s}}{1 + k_S C_e^{m_s}} \tag{7}$$

where q_S (mg/g) and k_S ($(dm^3/mg)^{1/m_S}$) are the Sips constants representing the monolayer adsorption capacity and m_S is an empirical constant.

RESULTS AND DISCUSSION

Characterization of the Materials. The powder X-ray diffraction pattern showed that purified saponite was a very pure sample. In fact, only a very weak maximum due to quartz emerged at $2\theta = 26.7°$ (see Figure 2). Considering that quartz has very high reflectance power as compared with the clay, only traces of quartz were present in the solid.

DOI: 10.1021/acsami.5b01894
ACS Appl. Mater. Interfaces 2015, 7, 10853−10862

Table 1. Characteristic Parameters Determined by SAXS Model Analysis for Aqueous Suspensions of Saponite and Functionalized Derivatives

	q_{max} (nm^{-1})		Δq_{max} (nm^{-1})		N		d (nm)	
sample	dry	swollen	dry	swollen	dry	swollen	dry	swollen
SAP	4.29	2.86	0.62	[a]	6.9	[a]	1.46	2.19
SAP−APTS	3.95	3.41	1.07	0.61	3.7	5.59	1.59	1.84
SAP−CTAB	3.23	2.70	0.72	[a]	4.5	[a]	1.94	2.32
SAP−CTAB−APTS1	3.46	3.37	0.73	0.8	4.7	4.21	1.82	1.86
SAP−CTAB−APTS2	3.39	3.04	0.69	[a]	4.9	[a]	1.85	2.05

[a]These values could not be determined.

In all cases, functionalization increased the interlayer spacing of the clay, from 1.47 nm in the starting saponite to 1.84 and 1.81 nm in the CTAB- and APTS-functionalized solids, respectively. Saponite functionalization with both CTAB and APTS consecutively or simultaneously afforded basal spacing of 1.93 nm, regardless of the method used to incorporate the two molecules. This value was somewhat larger than the basal spacing in the samples SAP−CTAB and SAP−APTS.

The incorporation of CTAB groups into the clay may have proceeded by a cation exchange mechanism in which CTA^+ cations substituted the electric charge and balanced the cations of the clay. CTA^+ measure 25 Å in length.[20] In SAP−CTAB, the basal spacing of 1.84 nm (gallery height of 0.88 nm) suggested an arrangement close to a bilayer, where the ammonium groups tethered to the clay surface, and the alkyl chains lay almost parallel to the layers.[21] As for the incorporation of APTS into the clay, the APTS molecules may have intercalated into saponite in its original, unmodified form, but they may also have undergone hydrolysis under the aqueous and acidic preparation conditions, which hydrolyzed the three ethoxy groups of APTS to hydroxyls. For the non−hydrolyzed molecule, the main dimension was close to 0.88 nm, which was compatible with the SAP−APTS sample (basal spacing of 1.81 nm, gallery height of 0.85 nm). However, APTS may also have adopted an almost planar configuration. In the case of SAP−CTAB−APTS1 and SAP−CTAB−ATPS2, both CTAB and ATPS might be located in the interlayer region, to increase the basal spacing by ca. 0.1 nm.

The small-angle X-ray scattering (SAXS) technique aided analysis of aqueous suspensions of pure saponite and of SAP−APTS, SAP−CTAB−APTS1, and SAP−CTAB−ATPS2. Platelets had dimensions in the order of a few hundred nanometers (Figure 3 and Table 1). SAXS evidenced the intralamellar structure of saponite from the equation $d = 2\pi/q_{max}$. All the dry solids had a well−defined structure, and their interlayer distance varied from 3.23 to 4.30 nm. The swelling experiments (suspension of clays in aqueous medium) affected the interlayer distance, and the changes agreed well with the X-ray diffraction results discussed above. The fact that q_{max} decreased and that d increased upon saponite functionalization confirmed clay swelling, attributed to the large distribution of d and to the lower stacking number, N, per crystal domain[22] (Table 1). This phenomenon was clear in the case of the intercalated derivatives SAP−CTAB and SAP−CTAB−APTS2. Natural and intercalated/grafted clays also had different q_{max} as a result of clay platelets swelling. The more marked difference in grafted clays stemmed from the higher concentration of organic units between the interlayer spaces. The intralamellar distance only changed in the clay swelled in the presence of water, and the peak position only depended on the concentration of the saponite/water suspension.

In their study of Na and Ca−montmorillonite, Segad et al.[23] observed that the platelet−platelet distance must be a linear function of the inverse of the clay volume in perfect lamellar clay−water systems; the slope must be equal to the thickness of a single platelet. However, these authors reported that d did not increase when the amount of water increased, because water addition to Ca−montmorillonite may have promoted extralamellar swelling between tactoids while keeping the interlamellar water layer constant. The intertactoid distance increased whereas the platelet−platelet distance remained unaltered. In our case, monitoring of a kinetic experiment from 30 s to 60 min by SAXS did not evidence any changes before clay platelets swelling by water in the interlayer cations. Hence, before the first layer of water occupied the interlayer clay platelets, longer water/saponite contact time did not promote any further clay expansion or swelling; in other words, the intralamellar distance remained the same. Figure 4 shows a schematic representation of the behavior of saponite and grafted/intercalated derivatives.

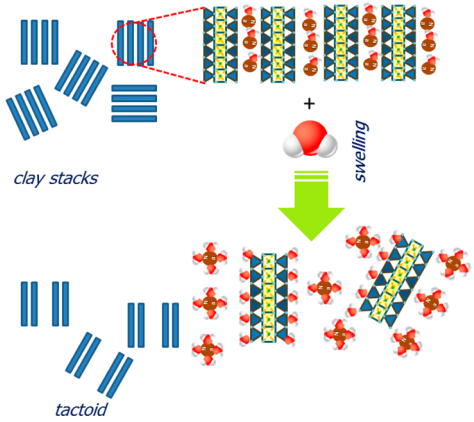

Figure 4. Schematic representation of the swelling of saponite and its grafted/intercalated derivatives in aqueous medium.

The FTIR spectra of the materials (Figure 5) revealed significant differences before and after clay functionalization with CTAB and APTS. First, the intensity of the sharp peak at about 3684 cm^{-1} markedly increased after functionalization. This peak is due to isolated hydroxyl groups attached to the octahedrally coordinated cations, mainly MgO−H. This intensification indicated that the hydroxyl groups interacted with the organic molecules during functionalization, probably via hydrogen bonding with the organic cations.[24] The bands at 2925, 2845, and 1474 cm^{-1}, attributed to CH antisymmetric and symmetric vibrations of the CH_2 species present in the functionalized materials, confirmed that APTS and CTAB functionalized the clay. These bands were more intense in the

DOI: 10.1021/acsami.5b01894
ACS Appl. Mater. Interfaces 2015, 7, 10853−10862

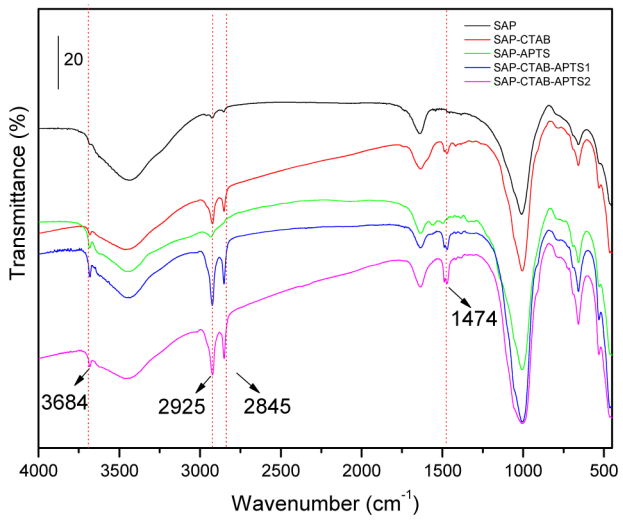

Figure 5. Infrared absorption spectra of the original and functionalized saponites.

solids containing CTAB, because this cation contains many more CH_2 groups. The intense band at 1008 cm^{-1}, due to Si−O−Mg−O−Si vibration, and the vibrations at lower wavenumbers, characteristic of M−O bonds (M = metal), did not change after clay functionalization and were similar for all the solids. It is worth remembering that the synthesis of APTS−containing solids required addition of HCl. Because saponite is very sensitive to acidic media, octahedral Mg^{2+} may have dissolved in the reaction medium, but this phenomenon did not seem to occur herein.

Thermogravimetric analysis of the original saponite (not shown) revealed two major mass losses: the first one (25−250 °C, 11%) corresponded to loss of water molecules adsorbed onto or intercalated into the clay mineral, whereas the second one (400−890 °C, 7%) resulted from saponite dehydroxylation. The DTA curves showed that the two processes were endothermic. DTA also evidenced an exothermic peak without any corresponding mass loss at 910 °C, ascribed to rearrangement of saponite to enstatite.[25]

SAP−APTS (see Figure 6a) underwent the same mass losses as the purified clay. The first mass loss was less intense, about 6%, due to removal of exchangeable cations and their hydration water. An extra mass loss split into two main stages occurred (192−670 °C, 11%). This suggested that the organosilane group may have decomposed in two steps, probably one that involved the amine part and another one that included the ethoxy groups or molecules located in different regions of the clay, such as the interlayer region and the surface of the layers. Unfortunately, it was not possible to analyze the gases and vapors that evolved during the decomposition and confirm which process actually took place.

SAP−CTAB (see Figure 6b) also experienced four major mass loss stages. The first stage happened between 25 and 150 °C and corresponded to only 4% of the initial mass of the solid. This loss might have been due to removal of the hydration water of the remaining exchangeable cations.[26] The second mass loss comprised two large effects centered at 300 and 600 °C. The first effect was actually composed of two effects and gave rise to various shoulders in the DTG curve, which suggested that CTAB existed in different parts of the solid. All these processes amounted to 21% mass loss. Considering that the purified saponite underwent 5% mass loss in this same temperature range, the remaining 16% may have resulted from CTAB decomposition.

The thermal curves recorded for SAP−CTAB−APTS1 and SAP−CTAB−APTS2 (see Figure 6c, d) resembled the curved obtained for SAP−APTS and especially the curve obtained for

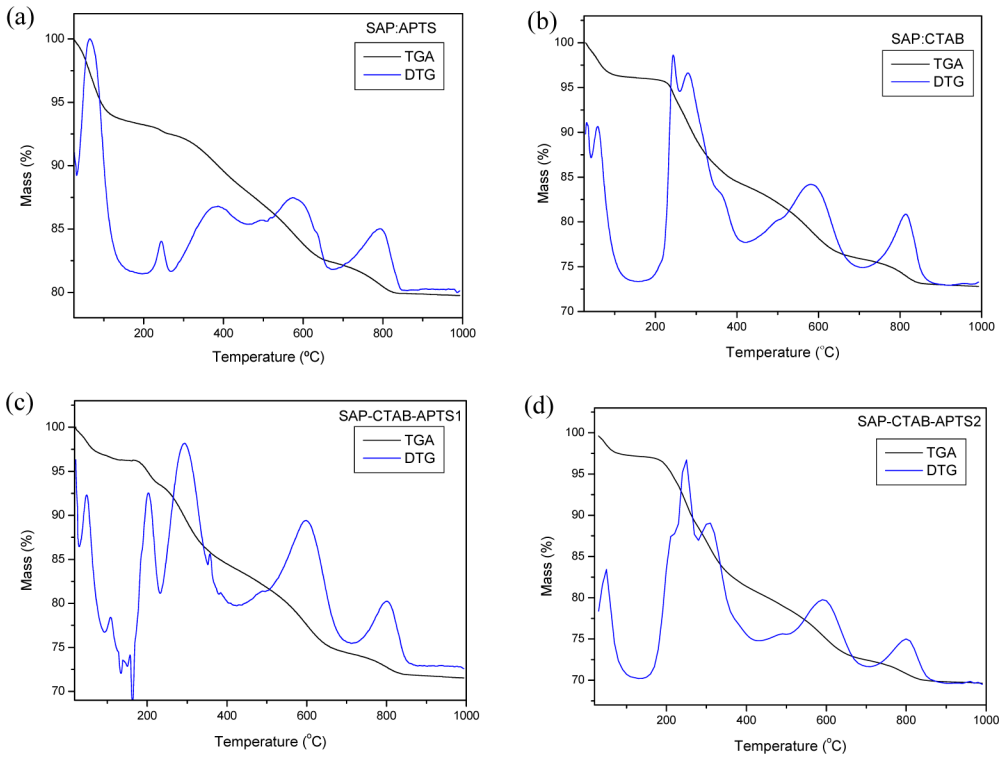

Figure 6. Thermal analysis of (a) SAP−APTS, (b) SAP−CTAB, (c) SAP−CTAB−APTS1, and (d) SAP−CTAB−APTS2.

DOI: 10.1021/acsami.5b01894
ACS Appl. Mater. Interfaces 2015, 7, 10853−10862

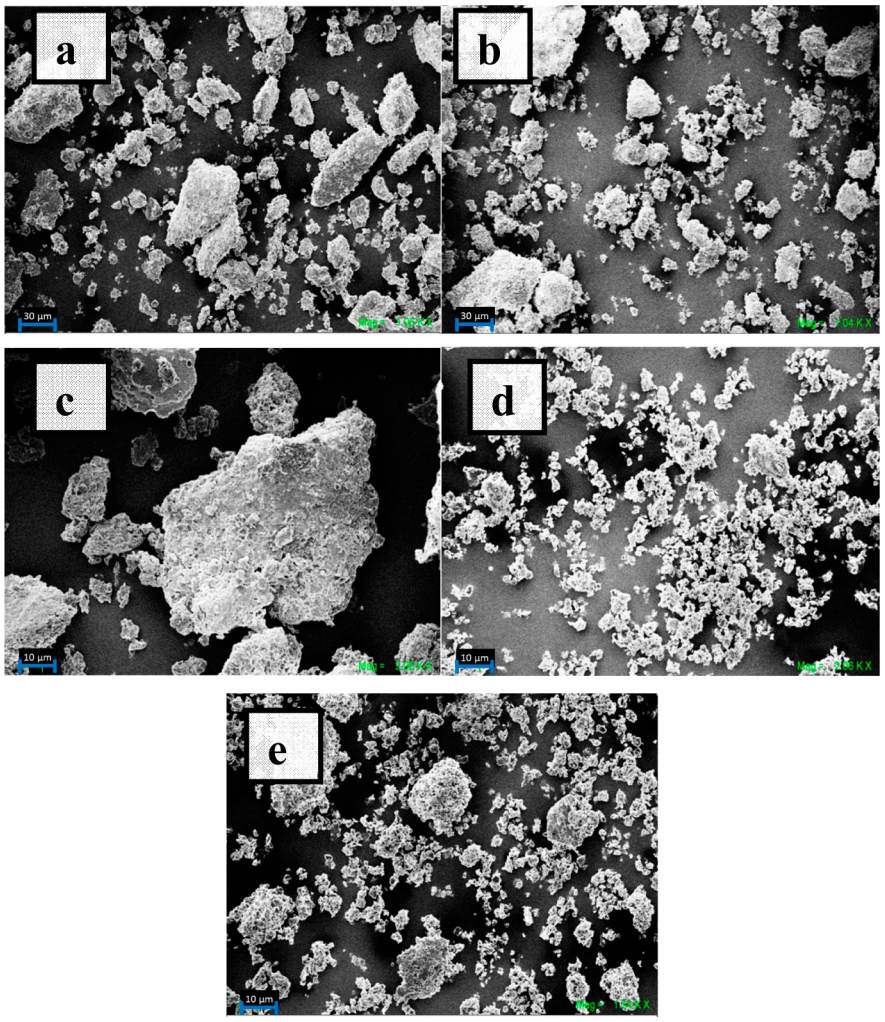

Figure 7. SEM micrographs of (a) SAP, (b) SAP−APTS, (c) SAP−CTAB, (d) SAP−CTAB−APTS1, and (e) SAP−CTAB−APTS2.

Table 2. Cation Exchange Capacity (CEC) and Specific Surface Area (SSA) Determined by the MB−Titration Method; Specific Surface Areas (S_{BET}) and Total Pore Volumes (V_{pTotal}) of Saponite and Its Functionalized Derivatives Were Calculated by the BET Method from N_2 Adsorption at −196 °C

sample	methylene blue volume saturation (cm^3)	CEC (mequiv/100 g)	SSA (m^2/g)	S_{BET} (m^2/g)	V_{pTotal} (cm^3/g)
SAP	17.5	35	273	77	0.097
SAP−APTS	2.5	5	39	160	0.138
SAP−CTAB	1.5	3	23	0.1	0.009
SAP−CTAB−APTS1	3.0	6	47	0.4	0.009

SAP−CTAB, suggesting that CTAB may have been preferentially fixed. Data from the TG curves (mass loss between 190 and 840 °C) helped to calculate the number of moles of APTS and/or CTAB per unit cell of saponite, which afforded the stoichiometry SAP−$(APTS)_{0.416}$ and SAP−$(CTAB)_{0.262}$. For the other materials, it was not possible to determine the stoichiometry because loss of the alkoxide and of the surfactant occurred in the same region.

The micrographs of the materials (Figure 7) showed that functionalization did not modify the saponite texture to a large extent, although the treated samples exhibited spongier particles. Particles disaggregated significantly, mainly in the SAP−CTAB−APTS1 solid, which displayed smaller particles than the other samples.

Table 2 lists the specific surface are and pore volume values obtained for all the materials via the N_2 adsorption method. APTS increased the S_{BET} of saponite from 77 to 160 m^2/g, while the materials containing CTAB had markedly smaller S_{BET}. Probably the bulk organic moieties (i.e., ammonium groups) blocked the access of N_2 molecules to the pores of the solids and hindered N_2 adsorption, in agreement with the findings reported by Silva and Airoldi.[27]

Table 2 also summarizes the CEC and SSA values calculated by means of the MB method. For all the solids, CEC drastically decreased after insertion of the organic units, which agreed with the fact that the organic cations substituted the originally existing cations in saponite. This phenomenon was particularly significant for SAP−CTAB, where the organofunctionalizing species was the hexadecyltrimethylammonium cation (the remaining CEC was only 3 mequiv/100 g), but it was also remarkable for SAP−APTS (residual CEC of 5 mequiv/100 g). For SAP−CTAB−ATPS, the residual CEC was slightly higher.

DOI: 10.1021/acsami.5b01894
ACS Appl. Mater. Interfaces 2015, 7, 10853−10862

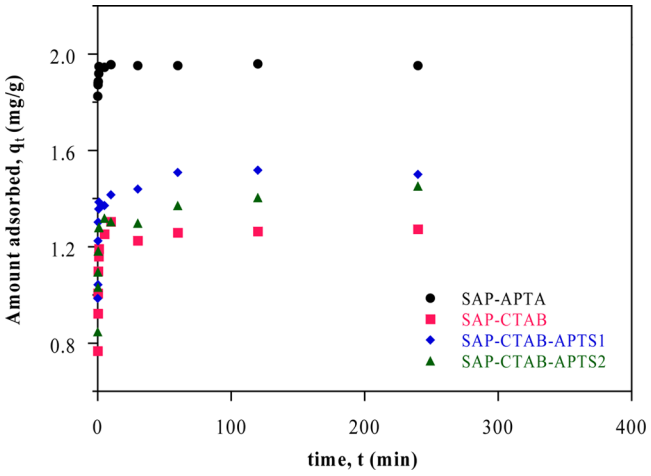

Figure 8. Kinetics data for caffeine adsorption on the investigated materials.

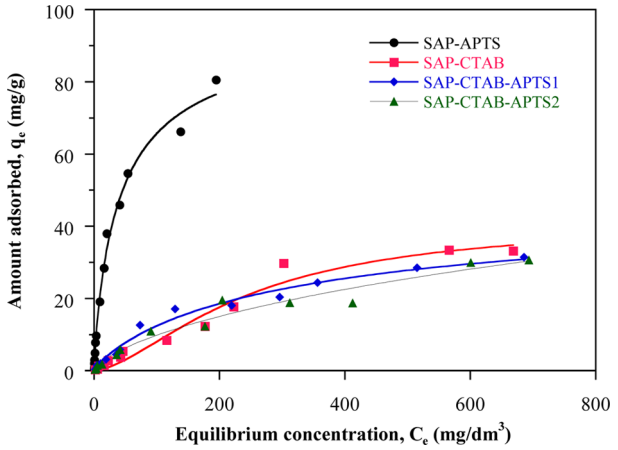

Figure 9. Equilibrium (symbols) and model (lines, Sips) isotherms for the equilibrium data for caffeine adsorption on modified saponites; 25 °C, pH 6.

Except for SAP−APTS, all the samples showed higher SSA values measured by the MB method as compared with the S_{BET} values measured by the N_2 adsorption method. For natural saponite, the tight bonding established between the layers when cations and water occupied the interlayer region hindered the access of nitrogen molecules during N_2 adsorption over dried samples. In contrast, the MB method, accomplished under wet conditions, allowed MB access to the entire clay surface. For the organofunctionalized saponites, the high occupancy of the interlayer region with CTAB and/or APTS species hindered the access of MB to this region, so the SSA measured by this method was much lower than that determined for saponite.

The differences between the N_2 and MB adsorption results were due to the different methodologies and intrinsic experimental conditions adopted in each case. The N_2 adsorption method only measured the external surface area (S_{BET}), while the MB adsorption method measured the internal and the external surface area (SSA). Maček et al. have recently underlined this difference by comparing the methods used to characterize soils via SSA measurement of clays. These authors reported that all the methods were indirect, and that the liquid used as adsorption agent and the mineral composition that determined the properties of every soil type strongly influenced these methods.[16] For example, the S_{BET} and SSA of a soil containing Ca−montmorillonite were 91.3 and 431 m^2/g, respectively. Smectite clays such as saponites can swell in the presence of water, which increases the basal spacing and favors the access of MB molecules, even though the latter molecules are larger than N_2 molecules. Because N_2 adsorption is not applied in solution, the MB method describes the exact surface of swollen clay better; i.e., it resembles the conditions employed during adsorption experiments.

Adsorption Experiments. *Kinetic Studies.* We evaluated the time that was necessary for each material to reach the equilibrium during the caffeine adsorption experiments by using 5.0 cm^3 of caffeine solution at 20 ppm and 50 mg of the adsorbent. On the basis of Figure 8, 240 min was the time of choice to conduct further adsorption assays involving different caffeine concentrations because all the systems had reached equilibrium before this time.

To examine the mechanism that controlled caffeine adsorption onto the investigated adsorbents, such as mass transfer in the solution and chemical reaction, it was necessary to test various kinetic models, such as the pseudo-first-order and pseudo-second-order models, to adjust the experimental data.[28] The following equation corresponds to the Largengren, or pseudo-first-order, equation

$$q_t = q_e[1 - \exp(-k_1 t)] \quad (8)$$

where k_1 (dm^3/min) is a first-order constant, q_t (mg/g) is the amount of caffeine adsorbed at time t (min), and q_e (mg/g) is the amount of caffeine adsorbed at the time that the equilibrium is reached.

Data analysis according to the pseudo-second-order model follows the equation

$$q_t = \frac{k_2 q_e^2 t}{1 + k_2 q_e t} \quad (9)$$

where k_2 (g/(mg min)) is a second-order adsorption constant.

The kinetic studies, Figure 8 and Table 3, revealed that the pseudo-second-order equation fitted the experimental data better, confirming that chemical adsorption controlled the process. The results indicated that the adsorption rate constants were proportional to the amount of caffeine adsorbed onto the clay. The calculated adsorption rate constants evidenced a higher value of caffeine adsorption onto the material SAP−APTS, 69.63 g/(mg min), attesting to the higher affinity of this matrix for caffeine.

Similar experiments conducted by using purified natural saponite as adsorbent showed that caffeine adsorption was negligible.

Table 3. Pseudo-Second-Order Equation Parameters for Caffeine Adsorption on the Modified Saponites

	SAP−APTS	SAP−CTAB	SAP−CTAB−APTS1	SAP−CTAB−APTS2
k_2 (g/(mg min))	69.63	10.45	12.12	9.63
χ^2	0.00043	0.0019	0.0028	0.00045
R	0.87	0.96	0.95	0.93

DOI: 10.1021/acsami.5b01894
ACS Appl. Mater. Interfaces 2015, 7, 10853−10862

Table 4. Freundlich, Langmuir, and Sips Equation Parameters for Caffeine Adsorption on the Modified Saponites

	SAP−APTS	SAP−CTAB	SAP−CTAB−APTS1	SAP−CTAB−APTS2
Freundlich				
K_F ($mg^{m_F+1}/(g\ dm^3)$)	7.6	0.41	0.98	0.64
m_F	2.2	1.4	1.9	1.7
χ^2	315	104	40	31
R	0.98	0.97	0.98	0.98
Langmuir				
Q_L (mg/g)	88	65	40	46
K_L (dm^3/mg)	0.031	0.0018	0.0046	0.0027
χ^2	87	74	26	29
R	0.995	0.98	0.992	0.98
Sips				
Q_S (mg/g)	97	42	48	68
K_S $(dm^3/mg)^{1/m_S}$	0.039	0.00014	0.0068	0.0044
m_S	0.87	1.61	0.86	0.80
χ^2	73	61	23	25
R	0.996	0.98	0.993	0.991

Equilibrium Experiments. To evaluate the efficiency of the prepared adsorbents, we studied equilibrium adsorption as a function of equilibrium concentration (Figure 9). In all cases, the adsorption capacity of the adsorbents increased with increasing initial caffeine concentrations; SAP−APTS had higher adsorption capacity than the other adsorbents. According to the Giles classification,[29] the shapes of the isotherms indicated L3-type behavior for SAP−APTS and L4-type behavior for SAP−CTAB, SAP−CTAB−APTS1, and SAP−CTAB−APTS2. L type or Langmuir isotherms have a convex, non-linear slope. In this case, the availability of the adsorption sites decreased with increasing solution concentration. According to this classification, the L3-type adsorbent, SAP−APTS, might present incompletely adsorbed caffeine layers, whereas the other solids, L4-type adsorbents, should have two complete layers of adsorbed caffeine, as confirmed by the fact that the isotherms reached a plateau.[30] All the materials adsorbed caffeine effectively. SAP−APTS afforded the highest adsorption: $q_{e(max)}$ = 80.54 mg/g; SAP−CTAB, SAP−CTAB−APTS1, and SAP−CTAB−APTS2 reached $q_{e(max)}$ values of 33.39, 31.43, and 30.63 mg/g, respectively. The simultaneous presence of both organic molecules in the clay did not favor adsorption. Indeed, SAP−CTAB−APTS1 and SAP−CTAB−APTS2 had lower adsorption capacities as compared with the materials that contained only one of the organic species. The more compact arrangement of both molecules in the clay seemed to impact the final adsorption capacity negatively. This result agreed with the report by Crini et al.,[31] who concluded that their adsorbents (chitosan-based materials) needed to have well-distributed active sites; in excess, these sites could hinder adsorption of target compounds. Non−linear regression (Table 4) helped to estimate the adsorption parameters for the solids evaluated in this work. The regression coefficients for the Freundlich, Langmuir, and Sips equations were higher than 0.97. The Sips isotherm model furnished the best fitting results. The estimated monolayer capacities, q_L and q_S, agreed with the experimental results.

CONCLUSIONS

CTAB and APTS were effectively incorporated into saponite, giving rise to functionalized clays. Clay modification was crucial to its performance as caffeine adsorbent. The saponite functionalized with APTS presented high affinity for caffeine, with maximum adsorption capacity of 80.54 mg/g after 4 h. The materials prepared herein are potential candidates for caffeine removal from aqueous solutions.

AUTHOR INFORMATION

Corresponding Authors

* Phone: +55 16 3711 8969. Fax:+55 16 3711 8878. E-mail: emerson.faria@unifran.edu.br.

*E-mail: katia.ciuffi@unifran.edu.br

Notes

The authors declare no competing financial interest.

ACKNOWLEDGMENTS

This work was carried out in the frame of a Spain−Brazil Interuniversity Cooperation Grant, financed by MEC (PHBP14/00003) and CAPES (317/15), and a Cooperation Grant from Universidad de Salamanca and FAPESP (2013/50216−0). Spanish authors thank additional financial support from Ministerio de Economía y Competitividad (MAT2013−47811−C2−R). We thank the Electronic Microscopy and Applied Chemical Analysis Services of NUCLEUS, University of Salamanca, for analysis of the samples. E.H. de Faria thanks the Brazilian Synchrotron Light Laboratory (LNLS) for providing beamtime at the D01ASAXS2 beamline and for assistance with the X−ray scattering experiments (Projects: SAXS 1/16981 and SAXS 1/17845) and FAPESP 2013/19523−3.

REFERENCES

(1) Bolong, N.; Ismall, A. F.; Salim, M. R.; Matsura, T. A Review of the Effects of Emerging Contaminants in Wastewater and Options for Their Removal. *Desalination* **2009**, *239*, 229−246.

(2) Barceló, D. Emerging Pollutants in Water Analysis. *Trends Anal. Chem.* **2003**, *22*, xiv−xvi.

(3) Kang, J.; Gu, H.; Zhong, L.; Hu, Y.; Liu, F. The pH Dependent Raman Spectroscopic Study of Caffeine. *Spectrochim. Acta, Part A* **2011**, *78*, 757−762.

(4) Buerge, I. J.; Poiger, T.; Müller, M. D.; Buser, H.−R. Caffeine, an Anthropogenic Marker for Wastewater Contamination of Surface Waters. *Environ. Sci. Technol.* **2003**, *37*, 691−700.

(5) Ogunseitan, O. A. Caffeine−inducible Enzyme Activity in *Pseudomonas putida* ATCC 700097. *World J. Microbiol. Biotechnol.* **2002**, *18*, 423−428.

DOI: 10.1021/acsami.5b01894
ACS Appl. Mater. Interfaces 2015, 7, 10853−10862

(6) Oller, I.; Malato, S.; Sánchez−Pérez, J. A. Combination of Advanced Oxidation Processes and Biological Treatments for Wastewater Decontamination−A Review. *Sci. Total Environ.* **2011**, *409*, 4141−4166.
(7) Worch, E. *Adsorption Technology in Water Treatment. Fundamentals, Processes, and Modeling*; De Gruyter: Berlin, 2012.
(8) Sotelo, J. L.; Rodríguez, A.; Álvarez, S.; García, J. Removal of Caffeine and Diclofenac on Activated Carbon in Fixed Bed Column. *Chem. Eng. Res. Des.* **2012**, *90*, 967−974.
(9) Sotelo, J. L.; Ovejero, G.; Rodríguez, A.; Álvarez, S.; Galán, J.; García, J. Competitive Adsorption Studies of Caffeine and Diclofenac Aqueous Solutions by Activated Carbon. *Chem. Eng. J.* **2014**, *240*, 443−453.
(10) Sotelo, J. L.; Rodríguez, A. R.; Mateos, M. M.; Hernández, S. D.; Torrellas, S. A.; Rodríguez, J. G. Adsorption of Pharmaceutical Compounds and an Endocrine Disruptor from Aqueous Solutions by Carbon Materials. *J. Environ. Sci. Health, Part B* **2012**, *47*, 640−652.
(11) Cabrera−Lafaurie, W. A.; Román, F. R.; Hernández−Maldonado, A. J. Transition Metal Modified and Partially Calcined Inorganic−Organic Pillared Clays for the Adsorption of Salicylic Acid, Clofibric Acid, Carbamazepine, and Caffeine from Water. *J. Colloid Interface Sci.* **2012**, *386*, 381−391.
(12) Cabrera−Lafaurie, W. A.; Román, F. R.; Hernández−Maldonado, A. J. Single and Multi−Component Adsorption of Salicylic Acid, Clofibric Acid, Carbamazepine and Caffeine from Water onto Transition Metal Modified and Partially Calcined Inorganic−Organic Pillared Clay Fixed Beds. *J. Hazard. Mater.* **2015**, *282*, 174−182.
(13) Okada, T.; Oguchi, J.; Yamamoto, K.; Shiono, T.; Fujita, M.; Iiyama, T. Organoclays in Water Cause Expansion that Facilitates Caffeine Adsorption. *Langmuir* **2015**, *31*, 180−187.
(14) de Faria, E. H.; Ciuffi, K. J.; Nassar, E. J.; Vicente, M. A.; Trujillano, R.; Calefi, P. S. Novel Reactive Amino−compound: Tris(hydroxymethyl)aminomethane Covalently Grafted on Kaolinite. *Appl. Clay Sci.* **2010**, *48*, 516−521.
(15) Hang, P. T.; Brindley, G. W. Methylene Blue Adsorption by Clay Minerals: Determination of Surface Areas and Cation Exchange Capacities (Clay−Organic Studies XVIII). *Clays Clay Miner.* **1970**, *18*, 203−212.
(16) Maček, M.; Mauko, A.; Mladenovič, A.; Majes, B.; Petkovšek, A. A Comparison of Methods Used to Characterize the Soil Specific Surface Area of Clays. *Appl. Clay Sci.* **2013**, *83*−*84*, 144−152.
(17) Freundlich, H. M. F. Over the Adsorption in Solution. *Z. Phys. Chem.* **1906**, *57*, 385−471.
(18) Langmuir, I. The Constitution and Fundamental Properties of Solids and Liquids. *J. Am. Chem. Soc.* **1916**, *38*, 2221−2295.
(19) Sips, R. On the Structure of a Catalyst Surface. *J. Chem. Phys.* **1948**, *16*, 490−495.
(20) Li, Z.; Jiang, W.−T.; Hong, H. An FTIR Investigation of Hexadecyltrimethylammonium Intercalation into Rectorite. *Spectrochim. Acta, Part A* **2008**, *71*, 1525−1534.
(21) Lagaly, G.; Ogawa, M.; Dékány, I. Clay Mineral−Organic Interactions. In: Bergaya, F., Lagaly, G. (Eds.), *Handbook of Clay Science, Part A: Fundamentals*, second ed.; Elsevier: Amsterdam, 2013; pp 435−505.
(22) Motokawa, R.; Endo, H.; Yokoyama, S.; Nishitsuji, S.; Kobayashi, T.; Suzuki, S.; Yaita, T. Collective Structural Changes in Vermiculite Clay Suspensions Induced by Cesium Ions. *Sci. Rep.* **2014**, *4*, 1−6.
(23) Ho, Y.−S. Review of Second−order Models for Adsorption Systems. *J. Hazard. Mater.* **2006**, *136*, 681−689.
(24) Segad, M.; Hanski, S.; Olsson, U.; Ruokolainen, J.; Akesson, T.; Jonsson, B. Microstructural and Swelling Properties of Ca and Na Montmorillonite: (In Situ) Observations with Cryo−TEM and SAXS. *J. Phys. Chem. C* **2012**, *116*, 7596−7601.
(25) Avila, L. R.; de Faria, E. H.; Ciuffi, K. J.; Nassar, E. J.; Calefi, P. S.; Vicente, M. A.; Trujillano, R. New Synthesis Strategies for Effective Functionalization of Kaolinite and Saponite with Silylating Agents. *J. Colloid Interface Sci.* **2010**, *341*, 186−193.
(26) Merchán, N.; Bañares−Munoz, M. A.; Vicente, M. A. Intercalation Compounds between Ethyl 2−oxocyclopentanecarboxylate and Saponite. *J. Inclusion Phenom.* **1998**, *31*, 219−230.
(27) Silva, C. R.; Airoldi, C. Acid and Base Catalysts in the Hybrid Silica Sol−Gel Process. *J. Colloid Interface Sci.* **1997**, *195*, 381−387.
(28) Xi, Y.; Mallavarapu, M.; Naidu, R. Preparation, Characterization of Surfactants Modified Clay Minerals and Nitrate Adsorption. *Appl. Clay Sci.* **2010**, *48*, 92−96.
(29) Giles, C. H.; Smith, D.; Huitson, A. A General Treatment and Classification of the Solute Adsorption Isotherm. I. Theoretical. *J. Colloid Interface Sci.* **1973**, *47*, 755−765.
(30) Falone, S. Z.; Vieira, E. M. Adsorption/Desorption of the Explosive Tetryl in Peat and Yellow−Red Argissol. *Quim. Nova* **2004**, *27*, 849−854.
(31) Crini, G.; Badot, P. Application of Chitosan, a Natural Aminopolysaccharide, for Dye Removal from Aqueous Solutions by Adsorption Processes using Batch Studies: A Review of Recent Literature. *Prog. Polym. Sci.* **2008**, *33*, 399−447.

DOI: 10.1021/acsami.5b01894
ACS Appl. Mater. Interfaces 2015, 7, 10853−10862